Eastern Mediterranean tectonics and tsunami hazard inferred from the AD 365 earthquake

B. SHAW[1]*, N. N. AMBRASEYS[2,3], P. C. ENGLAND[4], M. A. FLOYD[4], G. J. GORMAN[5], T. F. G. HIGHAM[6], J. A. JACKSON[1], J.-M. NOCQUET[7], C. C. PAIN[5] AND M. D. PIGGOTT[5]

[1]Bullard Laboratories, University of Cambridge, Madingley Road, Cambridge CB3 0EZ, UK
[2]Department of Civil Engineering, Imperial College, London SW7 2AZ, UK
[3]The Academy of Athens, Athens 10679, Greece
[4]Department of Earth Sciences, University of Oxford, Parks Road, Oxford OX1 3PR, UK
[5]Department of Earth Science and Engineering, Imperial College, London SW7 2AZ, UK
[6]Oxford Radiocarbon Accelerator Unit, University of Oxford, Oxford OX1 3QY, UK
[7]CNRS-Géosciences Azur, University of Nice, 250, Rue Albert Einstein, Valbonne, 06560, France
*e-mail: bs370@cam.ac.uk

Published online: 9 March 2008; doi:10.1038/ngeo151

Historical accounts describe an earthquake and tsunami on 21 July AD 365 that destroyed cities and drowned thousands of people in coastal regions from the Nile Delta to modern-day Dubrovnik. The location and tectonic setting of this earthquake have been uncertain until now. Here, we present evidence from radiocarbon data and field observations that western Crete was lifted above sea level, by up to 10 m, synchronously with the AD 365 earthquake. The distribution of uplift, combined with observations of present-day seismicity, suggest that this earthquake occurred not on the subduction interface beneath Crete, but on a fault dipping at about 30° within the overriding plate. Calculations of tsunami propagation show that the uplift of the sea floor associated with such an earthquake would have generated a damaging tsunami through much of the eastern Mediterranean. Measurement of the present rate of crustal shortening near Crete yields an estimate of ~5,000 yr for the repeat time of tsunamigenic events on this single fault in western Crete, but if the same process takes place along the entire Hellenic subduction zone, such events may occur approximately once every 800 yr.

The AD 365 earthquake was felt throughout the eastern Mediterranean, and its tsunami inundated coastal sites in Africa, the Adriatic, Greece and Sicily (Fig. 1). Rich agricultural land in the Nile Delta was abandoned as a result of the flooding, and previously populous hill cities were subsequently inhabited only by hermits[1] (see the Supplementary Information). Repetition of such an event would have catastrophic consequences for today's densely populated Mediterranean coastal regions.

The cause of the AD 365 event, and of other tsunamis in the Levant, such as those in AD 551 (ref. 2) and AD 1303 (ref. 3), has been enigmatic. Most of the world's devastating tsunamis are thought to be generated by slip on the interfaces between plates at subduction zones, but the Hellenic subduction zone, which is the only such major plate boundary of the region, seems to be largely aseismic[4].

The key to our study lies in a palaeoshoreline that fringes the coasts of western Crete and Antikythera, and was first described by Captain Spratt RN in 1851 (ref. 5). Spratt noted many 'sea marks' up to 10 m above present sea level in southwest Crete and, because these marks run through the remains of a Roman harbour at Phalasarna at 6 m above sea level, he deduced that the land must have been raised during or after the Roman era. Pirazzoli *et al.*[6] showed that this shoreline had a ^{14}C age of around 2,000 yr BP and attributed its uplift to an earthquake; this earthquake was subsequently linked to the AD 365 event[7–9].

RECENT SURFACE UPLIFT IN WESTERN CRETE AND ANTIKYTHIRA

Our first focus is to establish whether, as suggested previously, all of the recent uplift in western Crete indeed took place in one event, close to AD 365 . In what follows, we use the term 'uplift' to denote upward displacement of rocks relative to the geoid[10]. Because global sea level has been stable over the interval under consideration, we may take the present elevation of the palaeoshoreline as a proxy for such uplift.

A single prominent palaeoshoreline can be followed around the whole of western Crete; the algal encrustations marking this shoreline are not seen anywhere on the cliffs below this level, but similar constructions can be seen growing at sea level today. Previous radiocarbon dates of material from the upper levels of the palaeoshoreline were determined largely by conventional (non-accelerator mass spectrometry; AMS) methods and gave calibrated ages that lie within ~200 yr of AD 365 (refs 8,11). Taken together, these observations suggest that some uplift took place around AD 365, but they do not give direct evidence that the whole 10 m of uplift took place in one step, and the attribution of the uplift

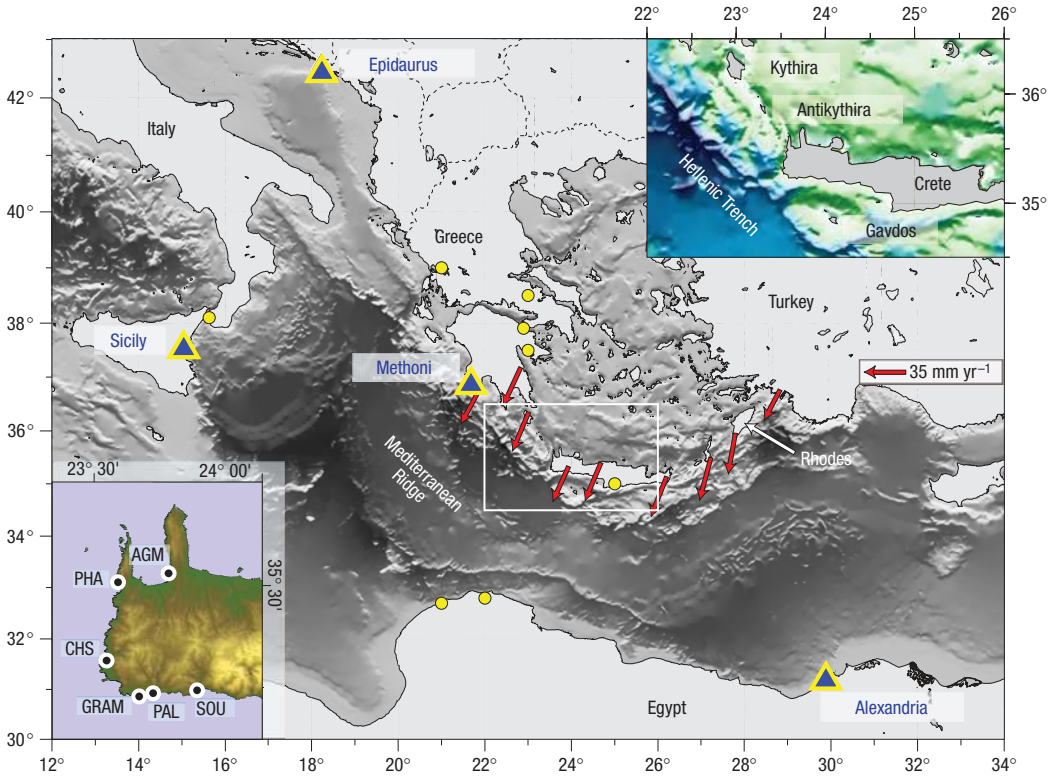

Figure 1 Location maps for this study. Yellow circles mark places where the AD 365 earthquake caused destruction, and blue triangles mark places affected by the associated tsunami. Red arrows show velocities of GPS stations near the Hellenic Trench relative to Africa, from ref. 47. The upper right inset shows the principal localities referred to in the text, and the prominent northwest–southeast bathymetric escarpment of the Hellenic Trench. The lower left inset shows the locations of samples for which radiocarbon dates are reported in Table 1.

to the AD 365 event was made uncertain by issues related to the calibration of the radiocarbon ages[12]. Here, we address both those sources of uncertainty with new, more accurate, radiocarbon dates on material from elevations between present sea level and the uplifted palaeoshoreline.

We collected corals, bryozoa and *Lithophaga* from widely separated locations in western Crete, at elevations between 1.5 m above sea level and the height of the palaeoshoreline. Everywhere we visited, the most recent colonizers seemed to be cheliostome bryozoa and ahermatypic corals, of which several had grown inside *Lithophaga* holes (see photos in the Supplementary Information). We obtained ^{14}C dates for 13 of these corals and bryozoa. For nine of them, calibrated AMS ^{14}C dates have 1σ ranges (typically $\sim\pm$70 yr) that include AD 365, and all but two of them include AD 365 in their 2σ age ranges (typically $\sim\pm$140 yr) (Table 1). All of the *Lithophaga* shells gave dates older than AD 365, presumably reflecting earlier colonization of the marine substrate, as we observed in the field.

Our new radiocarbon dates require that almost all of the uplift of western Crete took place within a few decades, that is, within the uncertainties of dating, of AD 365. (We have no datable material from locations lower than 1.5 m above sea level.) Although the data permit slow uplift during that interval, or uplift in a series of rapid small events, we shall show below that uplift of this magnitude in a single earthquake would have caused the historically recorded tsunami of AD 365 . Therefore, either the uplift of western Crete and its surrounding sea floor took place slowly within a few decades of AD 365 and some other event caused the tsunami that destroyed Alexandria in AD 365, or the two events are connected. In what follows, we assume the latter.

FAULT SLIP DURING THE AD 365 EARTHQUAKE

Measurements of ground displacements after an earthquake are commonly used to place bounds on the orientation and location of the fault that slipped. In the present case, such measurements are limited to uplift, in the sense defined above, of palaeoshorelines, and we use information from the distribution of earthquakes in the region as further constraints on the location of the fault that caused the AD 365 earthquake.

The most obvious candidate fault is the subduction interface, for which orientation and location are revealed by the focal mechanisms of earthquakes striking northwest–southeast at 40 km depth on a shallowly dipping ($\sim$15–20°) plane, directly below the southwest corner of Crete[13] (Fig. 2). This interface projects to the surface about 150 km southwest of Crete, where the Mediterranean Ridge, a prism of sediments $\sim$10 km thick, is deforming aseismically by folding and thrusting[14].

The distribution of shallow earthquakes (Fig. 2) suggests that other faults may be active in the region between the Mediterranean Ridge and the coast of Crete. The most prominent surface feature in this area is the Hellenic Trench, a linear northwest–southeast escarpment 3,500 m deep at its lowest point, 25 km southwest of Crete (Fig. 2). The proximity of this escarpment to the highest ground on Crete, where there is abundant geomorphological evidence of recent uplift, suggests that it marks the outcrop of a major reverse fault dipping beneath Crete. The Hellenic Trench strikes at 315°, parallel to the Mediterranean Ridge, and we therefore restrict our candidate faults for the AD 365 earthquake to faults with this strike and cropping out between the Mediterranean

Table 1 ^{14}C dates of samples from western Crete (identified by Oxford Radiocarbon Accelerator Unit sample number). Age ranges in bold include AD 365 (see the Methods section). Coral and bryozoa species were taken from or below the uplifted palaeoshoreline: S, *Stenocyathus vermiformus*; B, *Balanophyllia regia*; Ma, *Madracis pharensis*; My, *Myriapora truncata*; Ca, *Caryophyllidae* (sp.). The bivalves were taken from marine terraces at 20–24 m above sea level, and at least 10 m above the palaeoshoreline associated with the AD 365 event. Abbreviated location names correspond to the labels in the lower inset in Fig. 1: AGM, Agia Marina; PHA, Phalasarna; CHS, Chrisoskalitissa; GRAM, Gramena; PAL, Paleochora and SOU, Soughia.

Ox ID	Organism	Location	Height (m)	Top of palaeoshore (m)	^{14}C age BP	Calibrated age range (68.2% prob.)	Calibrated age range (98.4% prob.)
16743	coral (S)	PHA 1	3.5	6.6	1,985 ± 28	AD 415–546	**AD 340–604**
16745	coral (B)	PAL 8	9.0	9.0	2,019 ± 28	**AD 360–507**	**AD 282–565**
16991	coral (S)	PHA 3	3.0	6.6	2,032 ± 28	**AD 338–484**	**AD 271–551**
17669	bryozoa (My)	CHS 1	3.3	7.9	2,129 ± 27	**AD 238–378**	**AD 159–428**
17670	bryozoa (My)	CHS 2	3.0	7.9	2,071 ± 27	**AD 297–431**	**AD 235–515**
17671	bryozoa (My)	CHS 5	2.5	7.9	2,019 ± 27	**AD 360–506**	**AD 284–564**
17672	bryozoa (My)	CHS 5	2.5	7.9	2,024 ± 26	**AD 351–500**	**AD 280–556**
17673	coral (Ca)	CHS 7	6.0	7.9	2,345 ± 27	BC 22–AD 109	BC 100–AD 179
17674	coral (Ca)	AGM	3.0	5.5	1,977 ± 26	AD 423–550	**AD 352–608**
17675	bryozoa (My)	SOU NB2	2.2	6.7	2,119 ± 29	**AD 249–388**	**AD 166–438**
17676	bryozoa (My)	GRAM 2	4.7	9.0	1,878 ± 25	AD 539–653	AD 456–675
17677	bryozoa (My)	GRAM 4	2.0	9.0	2,015 ± 28	**AD 366–514**	**AD 288–570**
17678	coral (S)	PHA 2	3.4	6.6	2,028 ± 27	**AD 344–489**	**AD 275–553**
13809	bivalve	CHS T1	20–24	7.9	39,180 ± 300	41101–40661	41851–40327
14085	bivalve	CHS T2	20–24	7.9	37,700 ± 250	40615–39981	40649–39237
16995	bivalve	PAL T	20–24	9.0	47,300 ± 550	53063–45967	53461–45621

Ridge and the coast of Crete. This range bounds the plausible locations for reverse faults that could cause the observed uplift; a fault below the subduction interface is unlikely; a reverse fault cropping out on land would drop the southwestern-most part of Crete, not raise it.

We model slip on the candidate faults as planar dislocations buried within an elastic half-space[15]. We fix the strike of the faults at 315°; we did consider faults of other strikes, but found that they fit the data no better. We assume that relative motion was in the dip–slip sense, as seen in modern fault-plane solutions for the region; the uplift data, in any case, do not constrain the strike–slip component of motion. We assume that the fault slipped from the surface to a depth of 45 km, a depth suggested by the hypocentres of microearthquakes within the overriding plate, which are all shallower than 45 km (refs 16,17). This depth is also the maximum extent of shallowly dipping thrust faulting on the plate interface[13] (Fig. 2), as is common in subduction zones[18]. With these assumptions, the free parameters of the candidate faults are their end points, their dips and the amount of slip. We systematically searched this parameter space to find the fault that yielded the best fit (in the least-squares sense) to the observed uplift.

The best fit to the uplift data is obtained for a fault that crops out near the Hellenic Trench (Fig. 3). The fault length is 100 km, the slip is 20 ± 5 m to a depth of 45 km, the dip is 30 ± 5° and the r.m.s. misfit to the observations is 0.8 m (Fig. 3). The end points of the fault are constrained by uplift of 2.7 m on Antikythira in the northwest (of similar appearance and age to that on Crete[8,19]), and by the observation that there is no uplifted palaeoshoreline on the island of Gavdos, in the southeast. The trade-offs among parameters are illustrated in the Supplementary Information.

Slip on a fault that crops out at the Mediterranean Ridge is ruled out by the observations (see the Supplementary Information). If the causative fault is forced to have a dip as shallow (∼15°) as that of the plate interface, then the best-fitting solution, with an r.m.s. misfit of 0.9 m, yields a fault that crops out only 70 km southwest of Crete, where there is no obvious topographic expression of faulting. Any fault dipping at ∼15° requires slip of 40 ± 10 m to match the observed uplift (see the Supplementary Information), which is greater than has been recorded for any earthquake.

A previous model of the uplift[20] required a fault dipping at 40° to a depth of 70 km, well below the maximum seismogenic depth of 45 km beneath Crete. We have found solutions that allow slip to such a depth, but we regard them as unlikely to represent what occurred in the AD 365 earthquake, because they are generated only by the need to fit uplift of ∼2 m beyond 100 km from the southwest corner of Crete (Fig. 3c). Post-seismic relaxation after a thrust-faulting earthquake tends to cause uplift above the base of the co-seismic fault, and we regard it as more likely that the distant uplift is caused by post-seismic relaxation than by deep co-seismic slip. The data do not warrant a sophisticated analysis of post-seismic relaxation, but we have tested the plausibility of this suggestion by a combined co- and post-seismic calculation[21] in which the fault cuts through an upper, purely elastic, layer of 45 km thickness, that lies on a viscoelastic half-space. This calculation shows that 25 m of slip on the best-fitting fault, followed by complete viscous relaxation (for which case the viscosity of the half-space need not be specified), accounts better for the observations of uplift than our purely elastic model, particularly in its ability to fit the distant uplift of ∼2 m (Fig. 3d). (25 m, rather than 20 m, co-seismic slip is required because viscous relaxation causes subsidence close to the fault on the side of the fault that was uplifted in the earthquake.)

The parameters of the best-fitting dislocation solution allow us to estimate the minimum seismic moment for the AD 365 event. These parameters are equivalent to an earthquake of magnitude M_w 8.3–8.5. The ratio of slip (∼20 m) to length (∼100 km) for this fault is larger than normally observed[22], but the fault is similar in area and displacement to one of the maximum-slip fault patches in the M_w 9.3 Sumatra earthquake of 2004 (ref. 23) and to the 1897 Assam earthquake[24].

THE TSUNAMI

We carried out calculations of tsunamis using our best-fitting model of fault slip to provide initial conditions for the submarine surface displacement (see the Methods section). Figure 4 shows snapshots of the calculated sea surface height at times of 4 to 90 min after the earthquake, using the surface displacement

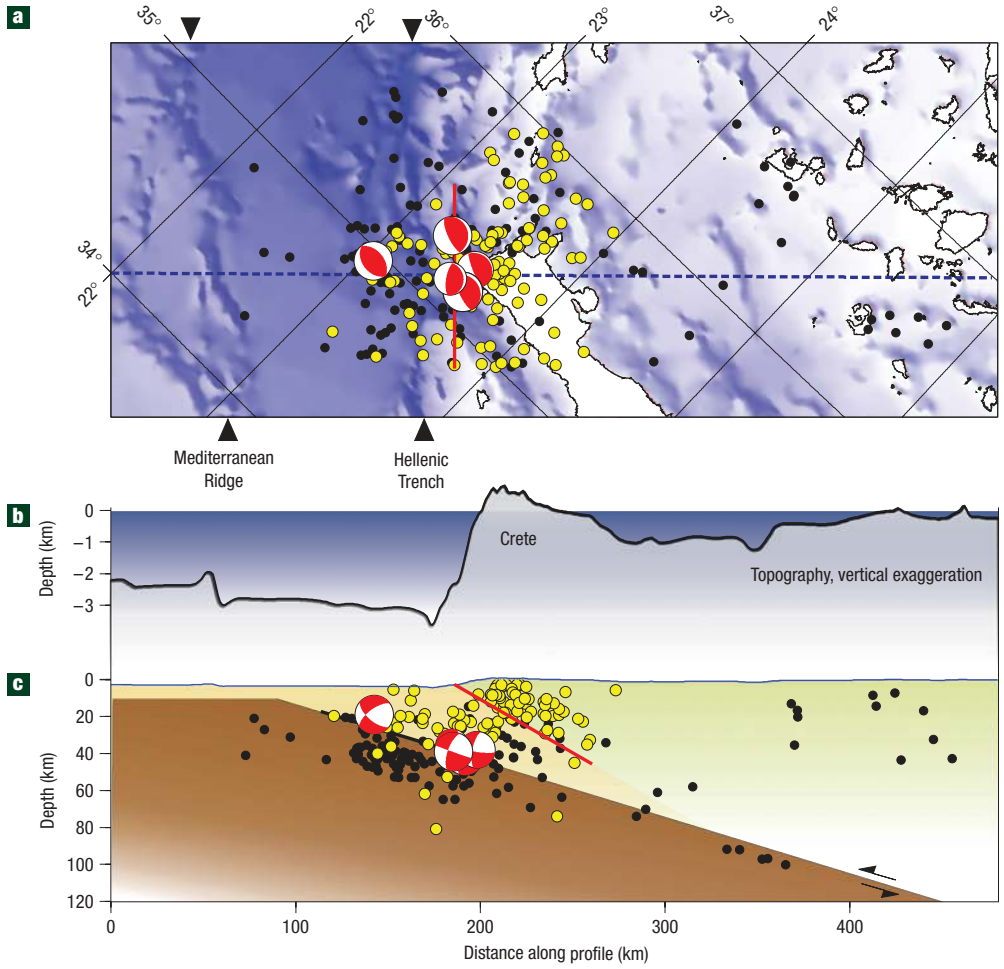

Figure 2 Seismicity and topography in the area of Crete. a, Seismicity of the region corresponding to the AD 365 earthquake. Black circles show epicentres of earthquakes determined from teleseismic data[48]; yellow circles show epicentres of microearthquakes determined from local networks[16,49,50]. Fault-plane solutions for earthquakes with well-determined depths on the plate interface are from ref. 13 and from this study. The best-fitting fault for the AD 365 earthquake (Fig. 3) is shown by a red line. **b**, Vertically exaggerated topography showing locations of the Mediterranean Ridge and Hellenic Trench. **c**, Topography and seismicity projected onto a vertical section along the dashed blue line in **a**, with our interpretation of the structure. The plate interface is shown by a black line and fault-plane solutions, and the best-fitting fault (Fig. 3) by a red line. Symbols for hypocentres as for epicentres in **a**.

pattern shown in Fig. 3 as the initial condition. The calculation shows that direct waves have the most significant effect, travelling towards the Nile Delta and up the Adriatic. The phases reflected off shorelines interfere, and become incoherent, in the relatively enclosed Mediterranean Basin (see Supplementary Information Movies S1a,b).

A prominent feature of the calculation is the wave sweeping east along the African coast to the Nile Delta (Fig. 4). In AD 365, the offshore island of Pharos (site of the famous lighthouse) was linked to the land by a causeway, the Heptastadion, which was vulnerable to the southwest and flooded by the tsunami. It was here that much destruction was concentrated.

Calculation of the sea surface height at a numerical 'tide gauge' situated in the mesh just off the shore of Alexandria shows wave heights of $\pm\sim 0.6$ m in the open ocean (Fig. 4f). There are many nonlinear effects of the detailed near-shore bathymetry that make it difficult to convert this range into an estimate of the run-up in ancient Alexandria, not least because local conditions of bathymetry and land surface have changed since AD 365. However, the open-ocean amplitude of the wave is comparable to that observed and modelled in the open ocean for the 2004 Sumatra tsunami[25], and we therefore presume that the onshore effects of such a sea wave would be devastating.

We also calculated the tsunami to be expected from 40 m of slip on the fault dipping at 15° (see Supplementary Information Movies S2a,b); the essential characteristics of this tsunami are very similar to those generated by the best-fitting fault, differing principally in that wave heights are greater by a factor of up to five. Even such large differences cannot reliably be resolved from the documented historical evidence and either modelled tsunami is compatible with what we know of AD 365 inundation, with the direct wave reaching all of the coastal sites described in historical records from the Nile Delta and North Africa to Sicily and the Adriatic, all of which are much more heavily populated now than at the time of the earthquake.

WHICH IS THE TSUNAMIGENIC FAULT BENEATH CRETE?

Assessment of the significance of the AD 365 earthquake hinges on understanding its role in accommodating the $\sim$35 mm yr^{-1}

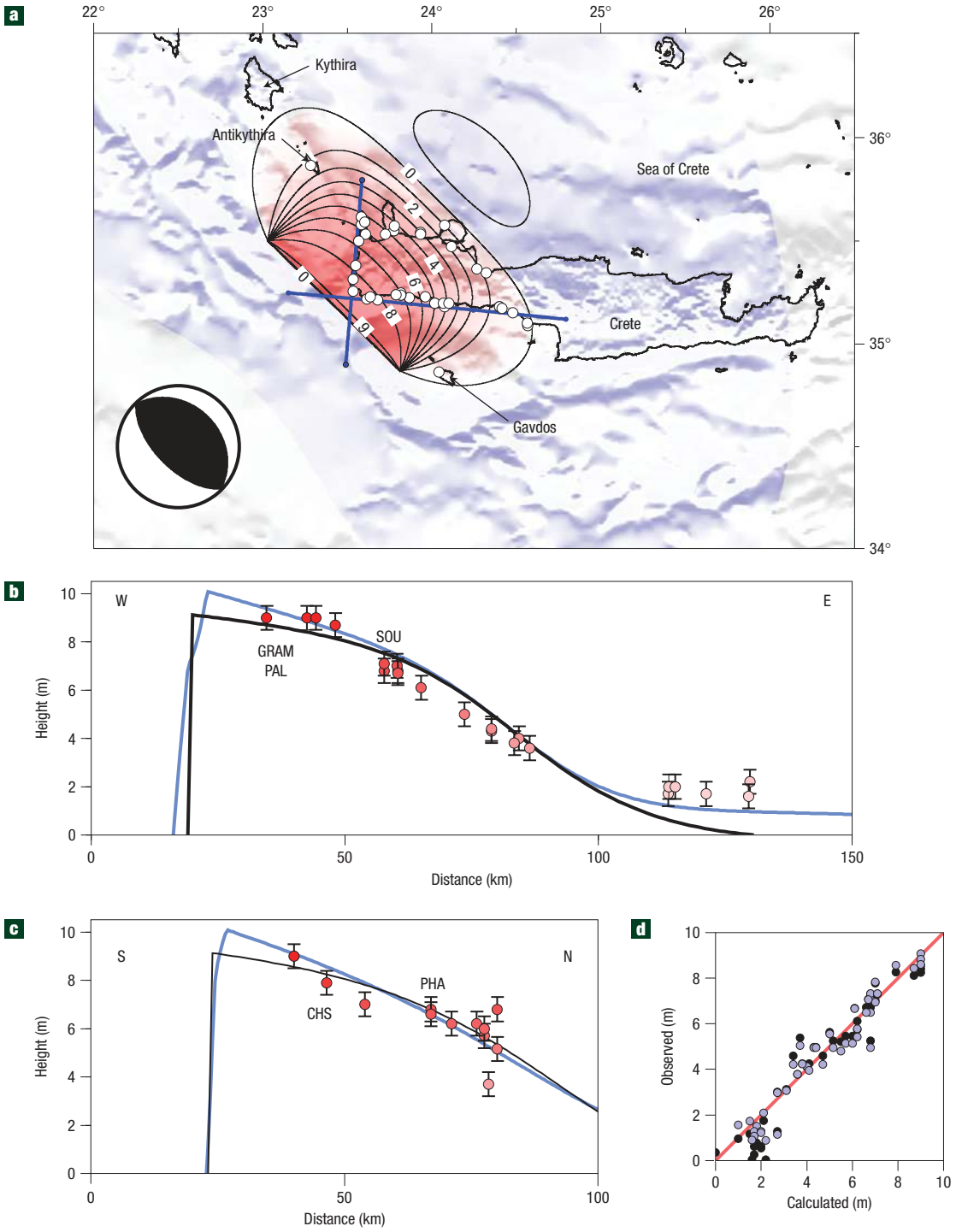

Figure 3 Observed and modelled uplift associated with the AD 365 earthquake. a, Contours of uplift calculated from the best-fitting elastic dislocation fault model, represented by the focal mechanism. White circles indicate sites of uplift observations on Crete, Antikythira and Gavdos. **b**, West–East profile of shoreline elevations along the south coast of Crete measured by refs 5,8 and ourselves, with 1 m error bars representing uncertainties arising from tidal range and measurement errors. The black line shows uplift calculated for the best-fitting elastic model for the earthquake; the blue line shows the calculation allowing for post-seismic viscous relaxation (see text). **c**, As for **b** but for South–North profile along the west coast. **d**, Observed and modelled elevations of palaeoshorelines for the best-fitting elastic dislocation model, with 20 m of slip (black circles) and for 25 m of slip, followed by complete post-seismic relaxation (blue circles).

of convergence between African and Eurasian lithosphere across the Hellenic subduction zone. Over the past hundred years (in which the record of earthquakes is, for this purpose, complete), earthquakes can account for no more than ~10% of that convergence[4], so we need to determine whether that percentage is representative of the longer term, or whether a significant fraction of the convergence is accommodated by rare, very large, earthquakes.

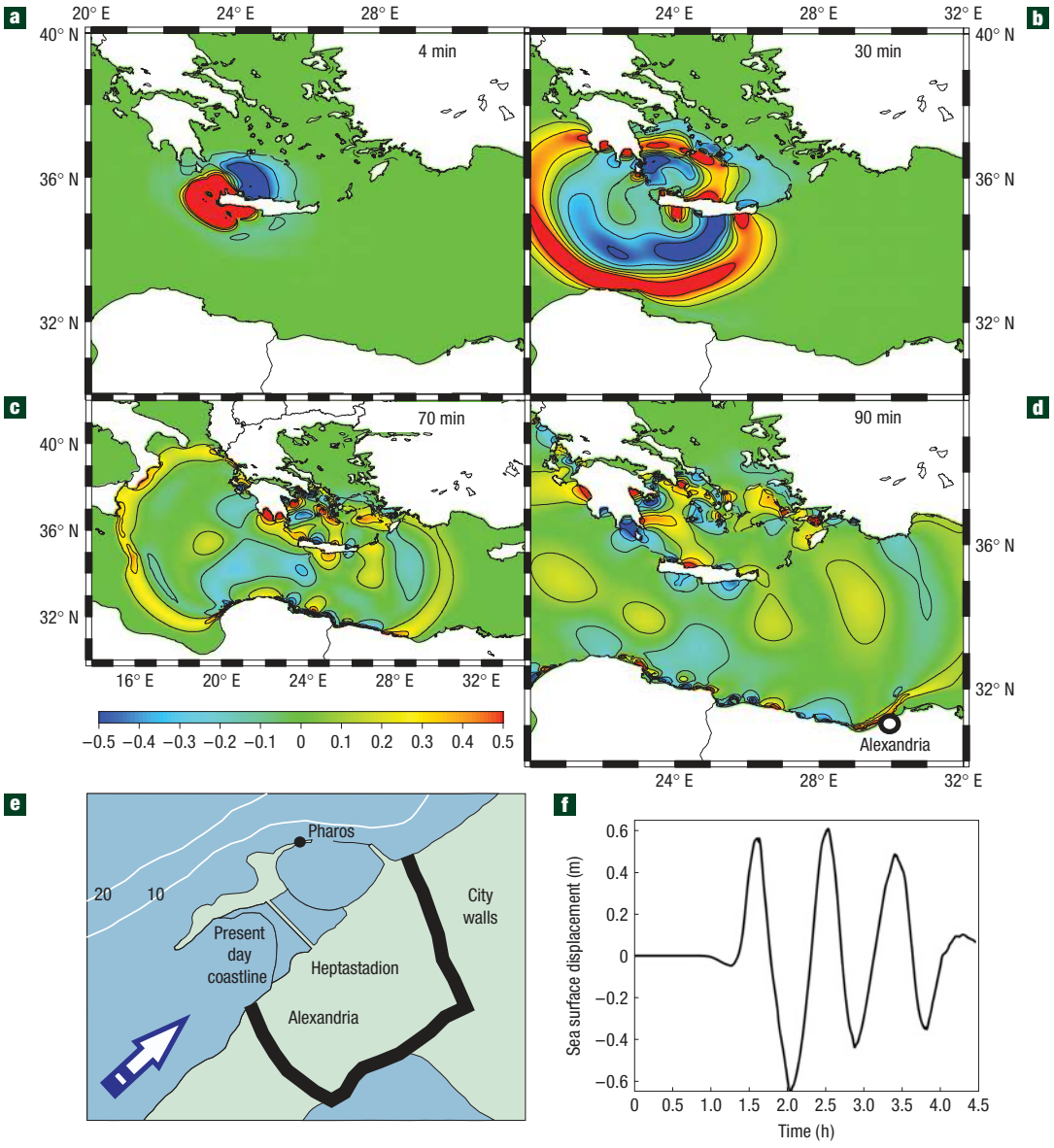

Figure 4 Tsunami calculation. a–d, Heights of the sea surface at 4, 30, 70 and 90 min after the earthquake. The direct wave travels to the North African coast and into the Adriatic, consistent with the historical record. **e**, A schematic map of Alexandria at the time of the 365 AD earthquake. The Island of Pharos was connected to the mainland by a narrow causeway, known as the Heptastadion, which was overtopped by the tsunami. Our calculations show that the wave would have arrived from the southwest (white arrow), explaining how the Heptastadion was inundated despite the apparent protection offered by Pharos Island against a direct wave from Crete, to the northwest. **f**, A plot of the wave height against time that would be observed in the open ocean off Alexandria in water of 20 m depth. The wave height would have been greatly amplified during run-up through shallower water towards the city.

If the long-term convergence took place principally in large earthquakes such as the AD 365 event then, in southwest Crete, such events would repeat approximately every 570 yr (for 20 m slip on the steeper fault) or every 1,140 yr (for 40 m slip on the plate interface). But field observations and radiocarbon dates show that the 2,000-yr-old palaeoshoreline was lifted close to its present position within a few decades of the AD 365 earthquake, implying that this was the only earthquake of significant size in that region in the past 1,650 yr. Nor, where the palaeoshoreline is preserved, is there evidence for previous AD 365-type events since sea level stabilized near its present height about 6,000 yr BP.

This argument can be extended to the whole Hellenic subduction zone, which is about 600 km long. To accommodate convergence across the whole zone seismically would require an earthquake equivalent to the AD 365 event every 100 to 200 yr. The historical record shows a small number of earthquakes in this region (two or three in the past 2,000 yr) that could have been of such magnitude but, although the record is incomplete, it is inconceivable that the 10–20 or more great earthquakes that would be needed to remove the deficit could have occurred unremarked. For these reasons, we conclude that most of the plate convergence in this region is aseismic[4]. This conclusion is reinforced by present-day global positioning system (GPS) measurements, which show that about 90% of the convergence rate is occurring by steady slip (see below).

On the other hand, the occurrence of a magnitude 8.3–8.5 earthquake means that strain must accumulate somewhere. There is

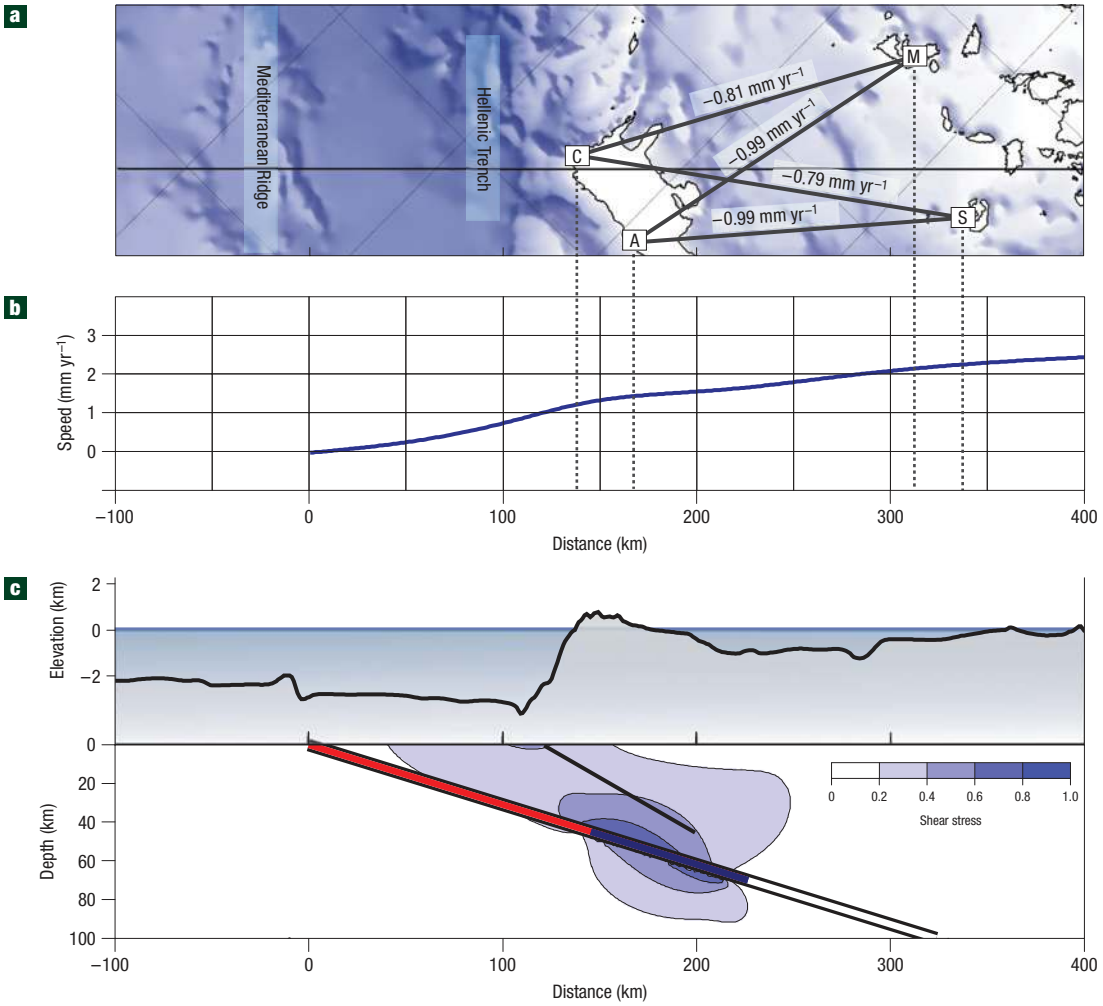

Figure 5 Schematic diagram of tectonic setting of the AD 365 earthquake. a, Continuous GPS data show shortening of ~1 mm yr^{-1} between Chrisoskalitissa (C) and Anopoli (A) in southern Crete and Milos (M) and Santorini (S), ~200 km to the northeast. **b**, Southwestward speed, calculated from model illustrated in **c**, of points within the Aegean, relative to the Mediterranean Ridge. **c**, Distribution of shear stresses calculated[15] for a planar fault, representing the interface between the African plate and the Aegean lithosphere, that slips 4 mm yr^{-1} more rapidly beneath 70 km (open line) than above 45 km (red line), with the slip varying linearly between those two depths (blue line). Relative values of shear stress are shown by the colour bar; absolute values, at any particular time, depend linearly on the slip difference that has accumulated between the two fault segments.

no known place where a fault that slips predominantly aseismically also fails in occasional great earthquakes, but a natural way to reconcile the accumulation of elastic strain with aseismic slip on the plate interface would be for that slip rate to be varying with depth. Variation in slip rate would cause strain to accumulate in the surrounding volume, which would eventually be released in an earthquake. One such variation is shown in Fig. 5, which shows that an increase in slip rate on the plate interface over the depth interval 45–70 km would cause compressional strain to accumulate beneath Crete.

Variation of slip rate with depth might result from a contrast in mechanical properties of different parts of the overriding plate, for instance between the accretionary prism of sediments and the continental crust of the Aegean. The combination of faulting we suggest may be common in subduction zone settings. A thrust fault has been imaged in the Nankai Trench off Japan at the landward edge of the accretionary prism[26,27] and slip on a similar fault is thought to have caused the 10 m uplift of Montague Island during the 1964 Alaska earthquake[28,29].

Repeated slip of the kind we propose for the AD 365 earthquake would cause permanent uplift of the surface of Crete by thickening the pile of sediments beneath it[30], and may account for the low seismic wave speeds beneath the island[31]. The contrast between the steep southern coast of Crete and its gentle northern slope (Fig. 2) is consistent with tilting by uplift on a fault cropping out near the south coast, so this proposed fault may control both the uplift and the extent of western Crete itself. Indeed, this geometry of faulting may be a common cause of long-term coastal uplift above subduction zones.

We conclude that the AD 365 earthquake took place by 20 m of slip on a fault ~100 km long, dipping northeast at 30° from the Hellenic Trench to a depth of 45 km. It has long been thought that slip along the plate interface between the Aegean and the Mediterranean ocean floor is predominantly aseismic. Our arguments here support that view but emphasize that the Hellenic Trench, which is a major feature along 400 km of the western coast of Greece, seems to mark the outcrop of a separate fault that is capable of producing rare, very large, tsunamigenic earthquakes

(see also ref. 9). We now attempt to assess the likelihood of a repetition of an event such as the AD 365 earthquake.

FUTURE TSUNAMIGENIC EARTHQUAKES

Measurements of relative motion across the southern Aegean using a continuous GPS network allow us to estimate the amount of elastic strain accumulating near the Hellenic Trench. Lines joining stations in western Crete to Milos and Santorini, about 200 km to the north, are shortening by approximately 1.6 mm yr^{-1} (Fig. 5a), with an uncertainty of about 0.1 mm yr^{-1} (see the Methods section). Such shortening is consistent with a slip deficit of ~4 mm yr^{-1} on the subduction interface (Fig. 5b); in other words, about 10% of the total convergence rate is being stored as elastic strain, with the rest being taken up by aseismic slip. At this rate, it would take ~5,000 yr to accumulate strain equivalent to the 20 m of slip that was released in the AD 365 earthquake. The predecessor of the AD 365 earthquake would then, plausibly, have happened more than 6,000 yr ago, when sea level was tens of metres below its present position[32].

Any direct evidence of uplift in an earthquake a few thousand years before 6,000 yr BP would now be submerged, but some support for this analysis comes from marine terraces at 20–24 m present elevation in western Crete, which three AMS ^{14}C dates place as having been formed 37–47,000 yr BP (Table 1), when the sea surface was ~75 m below its present level[32]. This observation independently suggests a long-term average uplift rate of ~2 mm yr^{-1}, which is consistent with uplift occurring in AD 365-type events that repeat every ~4,500 yr.

The processes described here for western Crete may also occur along the rest of the Hellenic subduction zone. The 1303 earthquake and tsunami are thought to have originated near Rhodes[1,33], so the whole Hellenic subduction zone may represent a tsunami hazard for the eastern Mediterranean. If the partitioning between aseismic and seismic slip is the same along the whole zone as in the 100 km section near southwest Crete, we should expect an AD 365-type earthquake every ~800 yr. That there has been only one other such event (in 1303) in the past 1,650 yr should focus our attention on the modern-day tsunami hazard in the Eastern Mediterranean.

METHODS

RADIOCARBON DATING OF MARINE ORGANISMS

Before treatment, the samples were examined under a scanning electron microscope to confirm the presence of primary structural fabrics. The cleanest pieces were selected for dating. All but four coral and bryozoan samples were thoroughly cleaned by shot blasting. Samples Phalasarna 1, Paleochora 8, Phalasarna 3 and Soughia 2 were cleaned ultrasonically in distilled water before being submerged in a bath of dilute (0.1 M) hydrogen peroxide until effervescence ceased.

Carbonate samples were dated using AMS ^{14}C dating at the Oxford Radiocarbon Accelerator Unit, University of Oxford. Samples of screened carbonate weighing 8–60 mg were ground in an agate pestle and mortar and hydrolysed *in vacuo* using a two-armed Pyrex reaction vessel with 2–3 ml of 100% ortho-phosphoric acid. Mass spectrometric analyses of the CO_2 were undertaken using a Europa ANCA Roboprep CHN analyser interfaced to a Europa 20/20 mass spectrometer operating in continuous-flow mode. Graphite was prepared by reduction of CO_2 over an iron catalyst in an excess H_2 atmosphere at 560 °C. AMS radiocarbon measurement was undertaken using the Oxford Radiocarbon Accelerator Unit 3MV Tandetron (High Voltage Engineering Europa)[34–37]. Radiocarbon ages were corrected for isotopic fractionation using the measured $\delta^{13}C$ values relative to the Vienna Pee Dee Belemnite standard.

Radiocarbon determinations were calibrated using the INTCAL04 Marine Calibration data set[38] and the OxCal computer calibration programme. A ΔR value of 53 ± 43 yr was used to account for the local reservoir offset (R) from the modelled world ocean[39]. This value is the average for the eastern Mediterranean region. The calibrated data are shown in Table 1.

The bryozoan sample Chrisoskalitissa 5 was analysed twice (17671,17672, Table 1) to check reproducibility. The 1σ and 2σ ages for samples 13809, 14085 and 16995 are years BC, and were obtained by comparing the radiocarbon ages with the ^{14}C record from the Cariaco Basin[40] with a 400 yr subtraction made from the conventional ages to account for the marine reservoir effect.

TSUNAMI MODELLING

The tsunami simulations were carried out with the Imperial College Ocean Model (http://amcg.ese.ic.ac.uk/ICOM; ref. 41). This model discretizes the Navier–Stokes equations in three dimensions and assumes the Boussinesq approximation. Finite-element discretization techniques are used on unstructured meshes, with the discretization and mesh formed in Cartesian coordinates on the surface of an assumed sphere of radius 6,378 km. The starting point for the tsunami simulation is the construction of an unstructured mesh representing the domain of interest. 1-min General Bathymetric Chart of the Oceans bathymetric data of the entire present-day Mediterranean Sea is optimized using Terreno (http://amcg.ese.ic.ac.uk/Terreno; ref. 42); the result is a one-element-deep tetrahedral mesh of approximately 2.8×10^5 nodes and 8.2×10^5 elements. No wetting/drying capability was used here, so the mesh stops at the 20 m bathymetric depth contour. A numerical tide gauge is placed at the edge of the mesh approximately 3 km offshore of Pharos. Crank–Nicolson time-stepping is used with a time-step of 30 s. Continuous piecewise-linear basis functions are used for the spatial discretization with a second-order anisotropic Smagorinsky large-eddy simulation turbulence model where the filter length scale depends on the local mesh size and shape.

Four Supplementary Information movies, at different zoom levels, show the propagation of the tsunami from the best-fitting fault model, and from a fault dipping at 15°, see also ref. 43.

CONTINUOUS GPS

The GPS stations whose data are used here are part of a network of 20 continuous stations run by the National Technical University of Athens and the University of Oxford. Daily solutions were obtained for this network, and for a network of selected continuous GPS sites in Eurasia, using GAMIT software[44]. Daily solutions were aligned with the International Terrestrial Reference Frame, 2005 (ref. 45) using GLOBK[46] to produce time series. For each time series, a linear trend, annual plus semi-annual periodic signals, and offsets associated with major receiver or antenna equipment changes were estimated assuming a white plus flicker noise model. Weighted r.m.s. residuals to the fit are <2 mm. Positions for the four stations used here are available from mid-2004 to mid-2007, yielding 807 measurements for the baseline from Anopoli (Fig. 5) to Milos, 997 from Chrisoskalitissa to Santorini, 780 for Anopoli to Santorini, and 1,007 for Chrisoskalitissa to Milos. Rates of contraction of the baselines are ~0.8–1.0 mm yr^{-1}, with associated realistic uncertainties less than, or equal to, 0.16 mm yr^{-1}.

Received 8 October 2007; accepted 12 February 2008; published 9 March 2008.

References

1. Ambraseys, N. N., Melville, C. P. & Adams, R. D. *The Seismicity of Egypt, Arabia and the Red Sea: A Historical Review* (Cambridge Univ. Press, Cambridge, 1994).
2. Elias, A. *et al.* Active thrusting offshore Mount Lebanon: Source of the tsunamigenic AD 551 Beirut-Tripoli earthquake. *Geology* **35**, 755–758 (2007).
3. Salamon, A., Rockwell, T., Ward, S. N., Guidoboni, E. & Comastri, A. Tsunami hazard evaluation of the Eastern Mediterranean: Historical analysis and selected modeling. *Bull. Seismol. Soc. Am.* **97**, 705–724 (2007).
4. Jackson, J. & McKenzie, D. The relationship between plate motions and seismic moment tensors, and rates of active deformation in the Mediterranean and Middle East. *Geophys. J+* **93**, 45–73 (1988).
5. Spratt, T. A. B. *Travels and Researches in Crete* Vol. 2 (J. van Voorst, London, 1865).
6. Pirazzoli, P. A., Thommeret, J., Thommeret, Y., Laborel, J. & Montaggioni, L. F. Crustal block movements from Holocene shorelines: Crete and Antikithera (Greece). *Tectonophysics* **86**, 27–43 (1982).
7. Pirazzoli, P. A., Ausseil-Badie, J., Giresse, P., Hadjidaki, E. & Arnold, M. Historical environmental changes at Phalasarna harbour, West Crete. *Geoarcheology* **7**, 371–392 (1992).
8. Pirazzoli, P. A., Laborel, J. & Stiros, S. C. Earthquake clustering in the Eastern Mediterranean during historical times. *J. Geophys. Res.* **101**, 6083–6097 (1996).
9. Papazachos, B. C. Large seismic faults in the Hellenic arc. *Ann. Geofis.* **39**, 891–903 (1996).
10. England, P. & Molnar, P. Surface uplift, uplift of rocks, and exhumation of rocks. *Geology* **18**, 1173–1177 (1990).
11. Thommeret, Y., Thommeret, J., Laborel, J., Montaggioni, L. F. & Pirazzoli, P. A. Late Holocene shoreline changes and seismo-tectonic displacements in western Crete (Greece). *Z. Geomorphol.* **40**, 127–149 (1981).
12. Price, S., Higham, T., Nixon, L. & Moody, J. Relative sea-level changes: reassessment of radiocarbon dates from Sphakia and west Crete. *Annual—British School at Athens* **97**, 171–200 (2002).

13. Taymaz, T., Jackson, J. & Westaway, R. Earthquake mechanisms in the Hellenic Trench near Crete. *Geophys J. Int.* **102**, 695–731 (1990).
14. Mascle, J. & Chaumillon, E. An overview of Mediterranean Ridge collisional accretionary complex as deduced from multichannel seismic data. *Geo-Mar. Lett.* **18**, 81–89 (1998).
15. Okada, Y. Internal deformation due to shear and tensile faults in a half space. *Bull. Seismol. Soc. Am.* **82**, 1018–1040 (1992).
16. De Chabalier, J. B. *et al.* A detailed analysis of microearthquakes in western Crete from digital three-component seismograms. *Geophys. J. Int.* **110**, 347–360 (1992).
17. Meier, T., Rische, M., Endrun, B., Vafidis, A. & Harjes, H.-P. Seismicity of the Hellenic subduction zone in the area of western and central Crete observed by temporary local seismic networks. *Tectonophysics* **383**, 149–169 (2004).
18. Tichelaar, B. W. & Ruff, L. J. Depth of seismic coupling along subduction zones. *J. Geophys. Res.* **98**, 2017–2038 (1993).
19. Pirazzoli, P. A. The early Byzantine tectonic paroxysm. *Z. Geomorphol.* **62**, 31–49 (1986).
20. Stiros, S. C. & Drakos, A. A fault model for the tsunami-associated, magnitude ≥8.5 Eastern Mediterranean, AD 365 earthquake. *Z. Geomorphol.* **146**, 125–137 (2006).
21. Wang, R., Lorenzo-Martin, F. & Roth, F. PSGRN/PSCMP-a new code for calculating co- and post-seismic deformation, geoid and gravity changes based on the viscoelastic-gravitational dislocation theory. *Comput. Geosci.* **32**, 527–541 (2006).
22. Scholz, C. H, Aviles, C. A. & Wesnousky, S. G. Scaling differences between large interplate and intraplate earthquakes. *Bull. Seismol. Soc. Am.* **76**, 65–70 (1986).
23. Subarya, C. *et al.* Plate-boundary deformation associated with the great Sumatra-Andaman earthquake. *Nature* **440**, 46–51 (2006).
24. Bilham, R. & England, P. Plateau pop-up in the great 1897 Assam earthquake. *Nature* **410**, 806–809 (2001).
25. Gower, J. Jason 1 detects the 26 December 2004 tsunami. *EOS trans. AGU* **86**, 37–38 (2005).
26. Park, J.-O., Tsuru, T., Kodaira, S., Cummins, P. R. & Kaneda, Y. Splay fault branching along the Nankai subduction zone. *Science* **297**, 1157–1160 (2002).
27. Moore, G. F. *et al.* Three-dimensional splay fault geometry and implications for tsunami generation. *Science* **318**, 1128–1131 (2007).
28. Plafker, G. Tectonic deformation associated with the 1964 Alaska earthquake. *Science* **148**, 1675–1687 (1965).
29. Ichinose, G., Somerville, P., Thio, H. K., Graves, R. & O'Connell, D. Rupture process of the 1964 Prince William Sound, Alaska, earthquake from the combined inversion of seismic, tsunami, and geodetic data. *J. Geophys. Res.* **112**, B07306 (2007).
30. Le Pichon, X. & Angelier, J. The Aegean Sea. *Phil. Trans. R. Soc. A* **300**, 357–372 (1981).
31. Endrun, B, Meier, T., Bischoff, M. & Harjes, H.-P. Lithospheric structure in the area of Crete constrained by receiver functions and dispersion analysis of Rayleigh phase velocities. *Geophys. J. Int.* **158**, 592–608 (2004).
32. Siddall, M. *et al.* Sea-level fluctuations during the last glacial cycle. *Nature* **423**, 853–858 (2003).
33. Hamouda, A. Z. Numerical computations of 1303 tsunamigenic propagation towards Alexandria, Egyptian Coast. *J. Afr. Earth Sci.* **44**, 37–44 (2006).
34. Bronk Ramsey, C. Radiocarbon calibration and analysis of stratigraphy: The OxCal program. *Radiocarbon* **37**, 425–430 (1995).
35. Bronk Ramsey, C. & Hedges, R. E. M. Hybrid ion sources: Radiocarbon measurements from microgram to milligram. *Nucl. Instrum. Methods B* **123**, 539–545 (1997).
36. Bronk Ramsey, C., Pettitt, P. B., Hedges, R. E. M., Hodgins, G. W. L. & Owen, D. C. Radiocarbon dates from the Oxford AMS system: Archaeometry Datelist 29. *Archaeometry* **42**, 243–254 (2000).
37. Bronk Ramsey, C., Higham, T. F. G. & Leach, P. Towards high precision AMS: Progress and limitations. *Radiocarbon* **46**, 17–24 (2004).
38. Hughen, K. A. *et al.* Marine04 marine radiocarbon age calibration, 0–26 cal kyr BP. *Radiocarbon* **46**, 1059–1086 (2004).
39. Reimer, P. J. & McCormac, F. G. Marine radiocarbon reservoir corrections for the Mediterranean and Aegean Seas. *Radiocarbon* **44**, 159–166 (2002).
40. Hughen, K., Southon, J., Lehman, S., Bertrand, C. & Turnbull, J. Marine-derived ^{14}C calibration and activity record for the past 50,000 years updated from the Cariaco Basin. *Quat. Sci. Rev.* **25**, 3216–3227 (2006).
41. Ford, R. *et al.* A nonhydrostatic finite-element model for three-dimensional stratified oceanic flows. Part I: Model formulation. *Mon. Weath. Rev* **132**, 2816–2831 (2004).
42. Gorman, G. J. *et al.* Optimal bathymetric representation through constrained unstructured mesh adaptivity. *Ocean Modell.* **12**, 436–452 (2006).
43. Fischer, K. D. & Babeyko, A. Modelling the 365 AD Crete earthquake and its tsunami. *Geophys. Res. Abs.* **9**, 09458 (2007).
44. Herring, T. A., King, R. W. & McClusky, S. C. *GAMIT Reference Manual: GPS Analysis at MIT, Release 10.3* (Department of Earth, Atmospheric, and Planetary Sciences, Massachussetts Institute of Technology, Cambridge, 2006).
45. Altamimi, Z., Collilieux, X., Legrand, J., Garayt, B. & Boucher, C. ITRF2007: A new release of the International Terrestrial Reference Frame based on time series of station positions and Earth Orientation Parameters. *J. Geophys. Res.* **112**, B09401 (2007).
46. Herring, T. A., King, R. W. & McClusky, S. C. *GLOBK Reference Manual: Global Kalman Filter VLBI and GPS Analysis Program, Release 10.3* (Department of Earth, Atmospheric, and Planetary Sciences, Massachussetts Institute of Technology, Cambridge, 2006).
47. Reilinger, R. *et al.* GPS constraints on continental deformation in the Africa-Arabia-Eurasia continental collisional zone and implications for the dynamics of plate interactions. *J. Geophys. Res.* **111**, B05411 (2006).
48. Engdahl, E. R., Van der Hilst, R. D. & Buland, R. P. Global teleseismic earthquake relocation with improved travel times and procedures for depth determination. *Bull. Seismol. Soc. Am.* **88**, 722–743 (1998).
49. Jost, M. L., Knabenbauer, O., Cheng, J. & Harjes, H.-P. Fault plane solutions of microearthquakes and small events in the Hellenic arc. *Tectonophysics* **356**, 87–114 (2002).
50. Hatzfeld, D., Besnard, M., Makropoulos, K. & Hatzidimitriou, P. Microearthquake seismicity and fault-plane solutions in the southern Aegean and its geodynamic implications. *Geophys. J. Int.* **115**, 799–818 (1993).

Acknowledgements

This work was supported by NERC, through grant NER/A/S/2001/01607 to P.C.E., and to COMET. M.D.P., G.J.G. and C.C.P. acknowledge the support of NERC under grants NE/C51829X/1 and NE/C52101X/1. We are indebted to H. Billiris, D. Paradisis and C. Raptakis for their support in the establishment and maintenance of the continuous GPS network whose results we use here, and to N. Forrest and M. Ziebart for many helpful discussions about processing continuous GPS data. We thank D. Hatzfeld for providing microearthquake data. We thank M. Brasier, N. Charnley, J. Darrell, O. Green, B. Rosen, P. Taylor, A. Thomas and the staff of the Oxford Radiocarbon Accelerator Unit, for their help in obtaining ^{14}C dates, with species identification and with sample preparation and imaging. We thank D. Ham for advice on computational modelling. We are grateful to R. Bilham, S. Lamb and P. Molnar for comments that improved the manuscript.
Correspondence and requests for materials should be addressed to B.S.
Supplementary Information accompanies this paper on www.nature.com/naturegeoscience.

Author contributions

N.N.A., P.C.E., J.A.J. and B.S. were involved in project planning. P.C.E., T.F.G.H., J.A.J. and B.S. carried out the field work and sampling. G.J.G., C.C.P. and M.D.P. are responsible for the tsunami modelling, and M.A.F. and J.-M.N. carried out the GPS analysis. T.F.G.H. is responsible for the radiocarbon dating. N.N.A. researched historical references to the earthquake.